Contents lists available at ScienceDirect

Applied Catalysis B: Environmental

Enhanced photocatalytic hydrogen production from glucose aqueous matrices on Ru-doped LaFeO$_3$

G. Iervolino [a], V. Vaiano [a,*], D Sannino [a], L. Rizzo [b], V. Palma [a]

[a] Department of Industrial Engineering, University of Salerno, Via Giovanni Paolo II, 132, 84084 Fisciano, SA, Italy
[b] Department of Civil Engineering, University of Salerno, Via Giovanni Paolo II, 132, 84084 Fisciano, SA, Italy

A B S T R A C T

In the present work, the renewable hydrogen production by the photocatalytic degradation of glucose over Ru-doped LaFeO$_3$ photocatalysts under UV or visible irradiation has been assessed for the first time. The perovskite doped with ruthenium was successfully synthesized by solution combustion synthesis. The effects on the hydrogen production and glucose degradation of reaction parameters, such as amount of ruthenium, initial concentration of glucose, reactor configuration and light source were systematically investigated. The results showed that the photocatalytic H$_2$ production from the glucose solution can be significantly enhanced (2179 μmol/g$_{cat}$ after 4 h of UV irradiation) using a specific amount of ruthenium (0.47 mol% of Ru) in LaFeO$_3$. Moreover, photocatalytic performances were strongly affected by reactor configuration; the comparison between two cylindrical reactors with different diameters showed improved performances in the reactor with the smaller diameter due to the enhanced photons flow that intercepts the photocatalysts particles dispersed into the glucose solution. In particular, under UV light, the hydrogen production increased from 2179 to 3474 μmol/g$_{cat}$ and the glucose degradation was complete after 3 h of irradiation.

Finally, the optimized photocatalyst was also tested under visible light on a real wastewater taken from a brewing process; the results showed an interesting hydrogen production as high as 2128 μmol/g$_{cat}$ (after 4 h of visible irradiation). In conclusion, this work further supports the interesting perspectives in the applicability of the photocatalytic process for the valorization of wastewater with the aim to obtain hydrogen from the degradation of target organic compounds.

© 2017 Elsevier B.V. All rights reserved.

1. Introduction

In recent years, the limited availability of fossil fuels and the increasing environmental pollution derived from their use as main source of energy has led to the development of new technologies for the production of zero environmental impact energy vectors such as hydrogen [1]. Hydrogen is a storable, clean and environmentally friendly fuel whose combustion results in the solely generation of water, with no emissions of atmospheric pollutants, greenhouse gases or particulates. However, about 95% of hydrogen currently derives from fossil fuels, mainly by steam reforming of natural gas and petroleum, while the remaining 5% comes from the electrolysis of water [2]. Because these processes involve the use of nonrenewable resources or high energy consumption, the corresponding routes of hydrogen production are not sustainable or economi-

cally feasible. Over the last few years, biomass, mainly glycerol, has been used to produce hydrogen by different methods, such as steam reforming [3], gasification [4], autothermal reforming [5] and electrochemical reforming [6]. Alternatively, hydrogen can be also produced from biomass in mild conditions (room temperature and atmospheric pressure) through heterogeneous photocatalysis [2].

Photocatalysis has been extensively studied for environmental remediation (i.e., pollutant degradation) and solar energy conversion (i.e., hydrogen production and CO$_2$ reduction) [7–15]. Up today, the photocatalytic production of hydrogen can be obtained mainly by two processes, i.e. either by the direct splitting of water into H$_2$ and O$_2$, or by the photo-reforming of organic compounds [16–22]. In many studies regarding the photocatalytic production of H$_2$, different substances (e.g., organic acids, alcohols, sulfide/sulfite) acting as electron donors, have been generally used [23–26]. However, this approach requires the use of sacrificial agents in order to get a good hydrogen production, which makes the process expensive. On the contrary, if the organic pollutants present in wastewater are seen as electron donors for H$_2$ produc-

tion, the overall process may be potentially cost-effective. Glucose is the most diffused and cheapest carbohydrate as it can be directly obtained from cellulose, the most abundant and renewable biomass on Earth. It is used for ethanol or butanol production, a wide variety of useful bio-based chemicals as industrial feedstocks for bioplastics and also to obtain hydrogen [27]. But glucose is also present at high concentration in wastewaters from some agro-food industries. Accordingly, the heterogeneous photocatalysis applied to wastewater treatment offers the opportunity to simultaneously recovery valuable products (such as hydrogen and methane) to be converted into energy [28–30]. Moreover, photocatalytic technology can be also operated under natural sunlight [31] so drastically cutting energy costs down. The most widely used semiconductor in photocatalysis is TiO_2 because of its physical and chemical properties, excellent stability, high availability and low cost [32]. With regard to the photocatalytic hydrogen production, the use of semiconductor (such as TiO_2 or ZnO) doped with nobles metals (Au, Pt, Pd) has been extensively reported [28,33–38]. Alternatively, $LaFeO_3$, one of the most common perovskite type oxide, has a general formula ABO_3, where position A is occupied by the rare earth ion (La^{3+}), and position B by the transition metal ion (Fe^{3+}). $LaFeO_3$ (conduction band potential = 0.025 eV [39]) has shown excellent photocatalytic activity because of its interesting properties such as high stability, non-toxicity and small band gap energy (2.07 eV), that qualify this perovskite as visible light active photocatalyst [40,41].

Generally, the functional properties of perovskite materials can be controlled either by modulating the crystalline structure or by the incorporation of different metal ions into the perovskite lattice [42]. $LaFeO_3$ powders doped with Sr and Cu have been recently tested in a photoelectrochemical process [42].

However, studies about the photocatalytic hydrogen production from aqueous solution on doped $LaFeO_3$ systems are still lacking in the literature. Among the several possible dopants for perovskites, ruthenium is the most suitable since a large amount of Ru^{3+} ions can be introduced within the perovskite network (in particular by replacing the transition metal cation of the perovskite) keeping it single-phase [43].

Therefore, in this work Ru-doped $LaFeO_3$ samples were synthesized and characterized and their effectiveness in the photocatalytic hydrogen production from glucose aqueous matrices has been assessed for the first time. The influences of Ru loading and photoreactor configuration have been analyzed. Finally, the optimized photocatalyst was also tested under visible light on a real wastewater taken from a brewing process.

2. Experimental

2.1. Synthesis of photocatalysts

Ru-$LaFeO_3$ samples were prepared by solution combustion synthesis, using citric acid as organic fuel and metal nitrate as metal precursor (oxidizer) [44]. In detail, 1.66 g of $Fe(NO_3)_3 \cdot 9H_2O$ (Riedel-deHaen, 97 wt%), 1.78 g of $La(NO_3)_3 \cdot 6H_2O$ (Fluka, 99%), 0.86 g of

citric acid (Fluka, 99 wt%) and a specific amount of $RuCl_3$ (Sigma Aldrich, 99%) used as dopant, were completely dissolved in 100 mL of bidistilled water. The solution was kept stirred continuously at 60 °C for 5 min. Then, ammonium hydroxide (Carlo Erba, 37 wt%) was slowly added to regulate the pH of the solution up to 7.0. The solution was dried at 130° C and then calcined at 300° C for 3 h in static air using a muffle furnace to ignite the solution combustion reaction [41]. Different amounts of $RuCl_3$ were used for the doping of $LaFeO_3$ to obtain photocatalysts with different amounts of Ru (Table 1). The Ru nominal loading is expressed as molar percentage and it was evaluated through Eq. (1):

$$\%molRu = \frac{nRu}{nLa + nFe} \cdot 100 \qquad (1)$$

Where: nRu is the number of moles of $RuCl_3$ used in the synthesis;

nLa is the number of moles of $La(NO_3)_3 \cdot 6H_2O$ used in the synthesis;

nFe is the number of moles of $Fe(NO_3)_3 \cdot 9H_2O$ used in the synthesis.

2.2. Photocatalysts characterization

Different techniques were used to characterize the photocatalysts. In particular the crystallite size and crystalline phase of Ru-$LaFeO_3$ photocatalysts were studied with an X-ray diffractometer (Assing), using Cu-Kα radiation. Total Ru content of the samples were determined by X-ray fluorescence spectrometry (XRF) in a thermoFischer ARL QUANT'X EDXRF spectrometer equipped with a rhodium standard tube as the source of radiation and with Si-Li drifted crystal detector. The specific surface area analysis was performed by BET method using N_2 adsorption with a Costech Sorptometer 1042 after a pretreatment at 150 °C for 30 min in He flow (99.9990%). The Raman spectra of the samples were recorded with a Dispersive MicroRaman system (Invia, Renishaw), equipped with 785 nm diode-laser, in the range 100–1000 cm^{-1} Raman shift. UV–vis reflectance spectra (UV-vis DRS) of powder catalysts were recorded by a Perkin Elmer spectrometer Lambda 35 using a RSA-PE-20 reflectance spectroscopy accessory (Labsphere Inc., North Sutton, NH). All spectra were obtained using an 8° sample positioning holder, giving total reflectance relative to a calibrated standard SRS-010-99 (Labsphere Inc., North Sut-ton, NH). Band-gap energy determinations of the photocatalysts were obtained from Kubelka–Munk function $F(R_\infty)$ by plotting $[F(R_\infty) \times h \nu]^2$ *vs.* h ν [45–47]. Scanning electron microscopy (SEM) (Assing, mod. LEO 420) was used to characterize the morphology of the samples at an accelerating voltage of 20 kV.

2.3. Photocatalytic tests

The photocatalytic experiments for hydrogen production from glucose aqueous matrices were carried out in a photocatalytic pyrex cylindrical reactor [10,48,49] (ID = 2.5 cm) (R1) equipped with a N_2

Table 1
Summary of the characterization results.

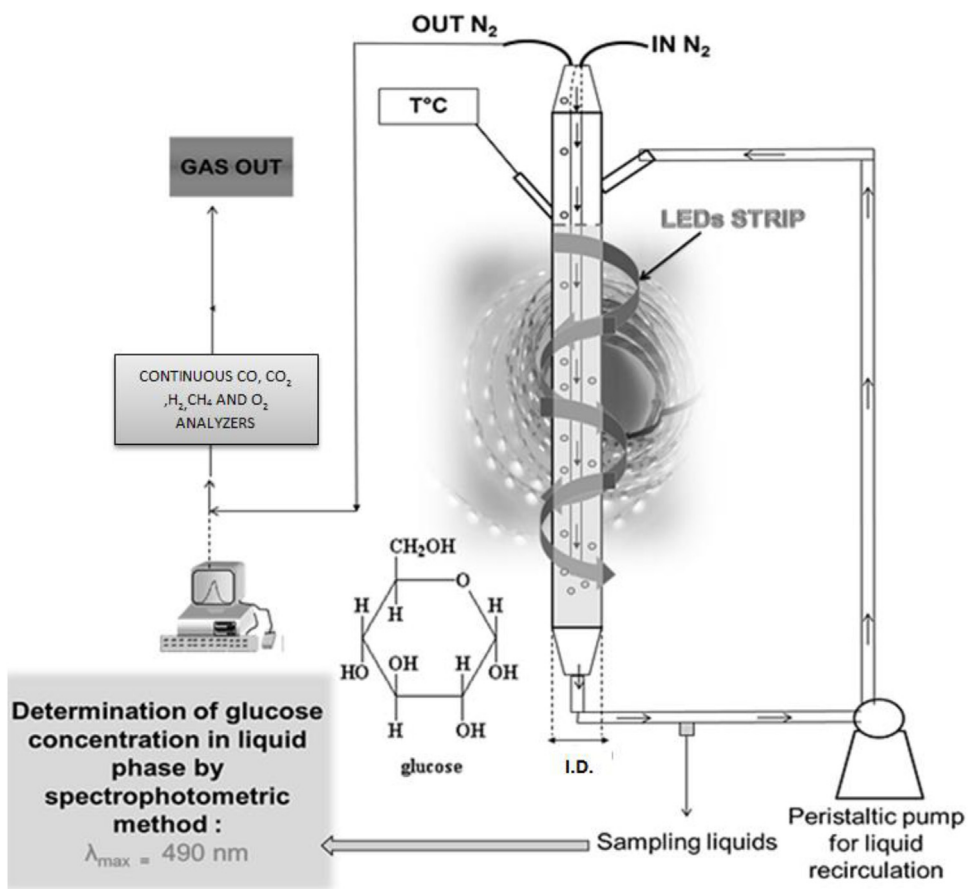| Catalyst	Ru nominal amount [mol%]	Ru measured amount (XRF) [mol%]	Crystallite size (XRD) [nm]	Specific surface area [m²/g]	Band gap (UV–vis DRS) [eV]
$LaFeO_3$	0	0	37	4	2.12
0.12% Ru	0.12	0.11	29	5	2.08
0.23% Ru	0.23	0.19	30	5	2.04
0.38% Ru	0.37	0.35	30	5	2.01
0.47% Ru	0.47	0.49	29	5	1.98
0.70% Ru	0.70	0.72	31	5	1.85
1.16% Ru	1.16	1.22	28	5	1.90
2.33% Ru	2.33	2.43	30	5	1.72

Fig. 1. Experimental set up for photocatalytic tests.

distributor device (Q = 0.122 NL/min) to assure the absence of O_2 during the tests. The experimental setup is represented in Fig. 1.

In a typical photocatalytic test, 0.12 g of the catalyst were suspended in 80 mL of an aqueous solution containing 1000 mg/L of glucose (D $^+$ Glucose VWR, Sigma-Aldrich). The pH of the solutions has not been changed and it was equal to about 6 for all the pho-

tocatalytic tests, corresponding to the spontaneous pH of glucose aqueous solutions. To ensure complete mixing of the solution in the reactor, a peristaltic pump was used. The photoreactor was irradiated with a strip of UV-LEDs (nominal power: 10W; light intensity: 57 mW/cm^2) with wavelength emission in the range 375–380 nm, or with a strip of visible LEDs with the main wavelength emission at
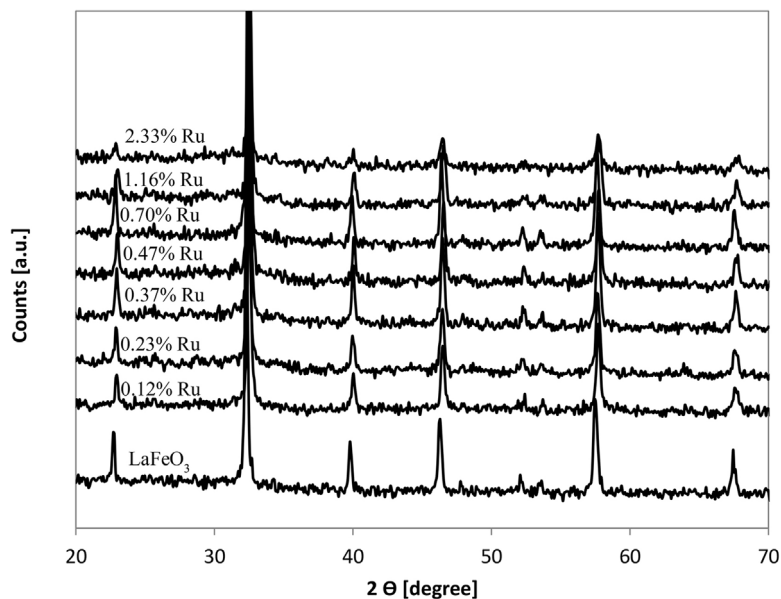

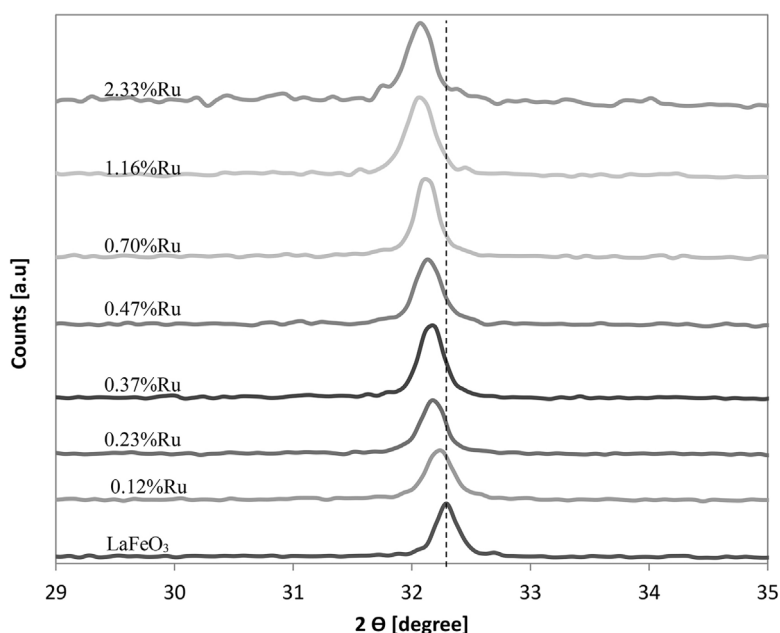**Fig. 2.** XRD spectra for undoped and Ru-doped LaFeO$_3$ in the range 20–70°.

Fig. 3. XRD spectra for undoped and Ru-doped LaFeO₃ in the range 29–35°.

about 460 nm (nominal power: 10 W; light intensity: 32 mW/cm^2). The LEDs strip was positioned around the external surface of the reactor so that the light source uniformly irradiated the reaction volume. The suspension was left in dark conditions for 2 h to reach the adsorption-desorption equilibrium of glucose on the photocatalyst surface, and then the reaction was started under UV (or visible) light up to 4 h. About 2 mL of sample were taken from the photoreactor at different times and filtered (filter pore size: 0.45 μm) in order to remove photocatalyst particles before the analyses. To evaluate the effect of reactor design, another photoreactor (R2) with a nominal volume equal to the first one (R1) but with an internal diameter equal to half (1.25 cm) was also investigated. Finally, to evaluate the effect on real wastewater containing glucose, the optimized photocatalyst was tested under visible light on a wastewater sample taken from a brewing process (pH: 6; total suspended solids: 450 mg/L, TOC: 1000 mg/L).

2.4. Chemical analysis

The characterization of the gaseous phase coming from the photoreactor was performed by continuous CO, CO_2, O_2, H_2 and CH_4 analyzers (ABB Advance Optima). The concentration of glucose was measured by a spectrophotometric method [50] at 490 nm using UV–vis spectrophotometer (Lambda 35, Perkin Elmer). According to the method, 2 mL of a carbohydrate solution was mixed with 1 mL of 5 wt% aqueous solution of phenol (Sigma-Aldrich) in a test tube. Subsequently, 5 mL of concentrated sulfuric acid (Sigma-Aldrich) was added rapidly to the mixture. The gluconic acid formed during the irradiation time was quantified by analyzing the UV absorption of liquid samples at 264 nm [26] using the same equipment. Leaching tests were carried out to check the release of La and Ru from the samples during the photocatalytic tests, analysing the solution by inductive coupled plasma-mass spectrometry (7500c ICP-MS, Agilent).
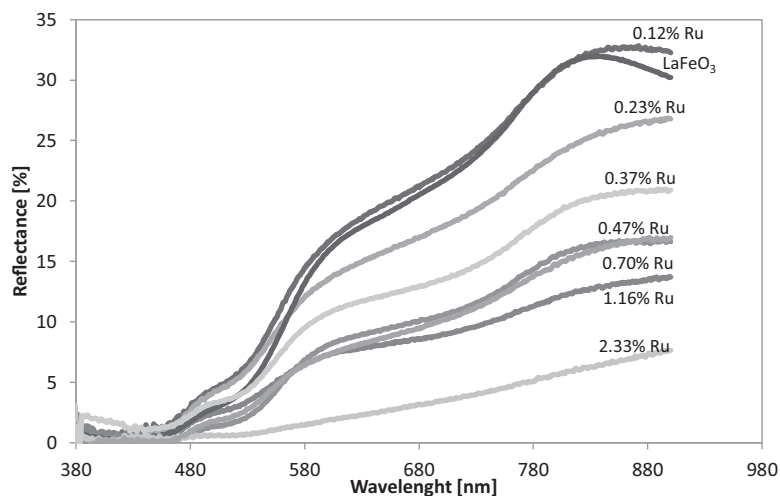

Fig. 4. UV Vis DRS spectra for undoped and Ru-doped LaFeO₃.

3. Results and discussion

3.1. Photocatalysts characterization

3.1.1. X-ray diffraction (XRD)

Fig. 2 shows the XRD patterns of the $LaFeO_3$ photocatalyst doped with different amounts of ruthenium. XRD showed well indexed diffraction peaks, clearly indicating the formation of orthorhombic perovskite type structure, as reported in literature [41,51]. Additional peaks due to ruthenium oxide were not observed up to a Ru loading of 1.16 mol%. In fact, for 1.16%Ru and 2.33%Ru catalysts, XRD patterns showed an additional diffraction peak at 2θ value of about 35° due to the presence of RuO_2 on the surface, indicating only a partial doping of perovskite structure [52].

XRD data in the range 29–35° (Fig. 3) also show that the peak of the X-ray diffraction at 32.2° of undoped $LaFeO_3$ shifted towards lower 2θ values for all the Ru-$LaFeO_3$ samples. The reason for this phenomenon is that the radius of Ru^{3+} (0.0820 nm) cation is larger than Fe^{3+} (0.0645 nm), which leads to the decrease of unit cell lattice parameter, according to literature for perovskite samples doped with ruthenium [53]. This last result indicates that Ru^{3+} cation partially substitutes Fe^{3+} cation in the perovskite structure.

The crystallite size of the samples was calculated by Scherrer formula for a diffraction line positioned at 2θ value of about 32° [51] (Table 1).

Comparing doped and undoped $LaFeO_3$, it can be observed that the doping process induced a slight decrease of photocatalysts crystallite size, though no clear relationship could be established between Ru contents. A similar result was previously observed for $SrTiO_3$ perovskite doped with Ru [53].

3.1.2. BET surface area and XRF results

BET surface area values (S_{BET}) of the catalysts are shown in Table 1. In agreement with XRD results, S_{BET} values did not change when Ru amount used in the catalyst preparation was increased. In particular, S_{BET} increased from 4 to 5 m^2/g for undoped $LaFeO_3$ and Ru-doped $LaFeO_3$, respectively. The total amount of Ru in the samples was determined by XRF (Table 1). In every case, the real Ru content well fits the nominal metal content indicating a good yield of the synthesis process.

3.1.3. UV–vis diffuse reflectance spectra

The reflectance spectra (Fig. 4) showed the typical absorption band edge of the $LaFeO_3$ semiconductor at around 814 and 600 nm for all the samples and it can be attributed to electron transitions from valence to conduction band ($O_{2p} \rightarrow Fe_{3d}$) [54]. It is worthwhile to note that these bands disappeared for the catalysts with the higher Ru content (1.16%Ru and 2.33%Ru). This result could be due to the presence of RuO_2 on the $LaFeO_3$ surface, observed in XRD measurements (Fig. 2).

The absorption edge of Ru-doped $LaFeO_3$ catalysts has a red shift and also a stronger absorption than the pure $LaFeO_3$ in the visible region. Similar results were observed for Li-doped $LaFeO_3$ samples [55].

The data obtained from UV–vis reflectance spectra were used for evaluating the band-gap energy of the photocatalysts (Fig. 5). The obtained results are reported in Table 1. The increase of Ru amount resulted in a decrease of band-gap energy from 2.12 (band-gap of undoped $LaFeO_3$) to 1.72 eV for 2.33%Ru. The decrease of band-gap energy was due to the electronic transition from donor levels formed with dopants to the conduction band of the host photocatalysts [56]. In our case, the dopant exist as a trivalent ion (Ru^{3+}) on the Fe^{3+} site, which forms a donor level at a lower potential than the top of the valence band composed of O 2p orbitals, and the apparent band-gap energy consequently became narrowed [56].
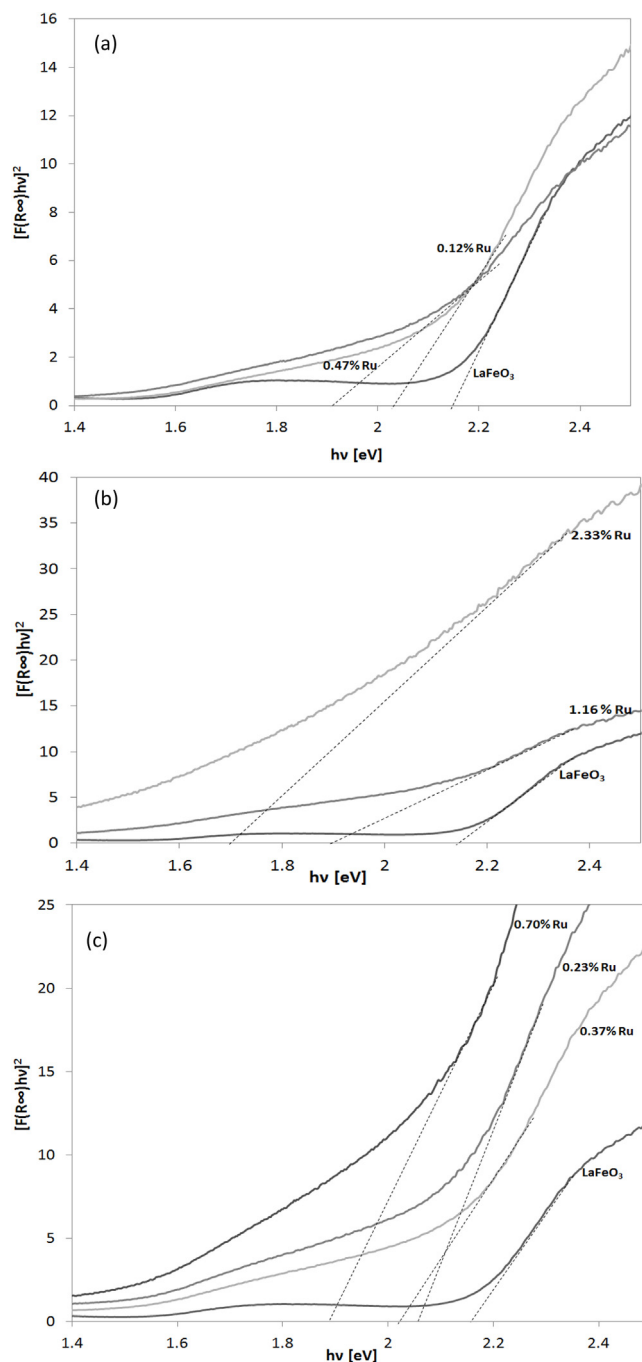

Fig. 5. Evaluation of band gap for undoped and Ru-doped $LaFeO_3$.

3.1.4. SEM analysis

The morphology of the $LaFeO_3$ and Ru-doped $LaFeO_3$ photocatalysts was investigated by SEM microscopy and the obtained results are presented in Fig. 6. For sake of brevity, together with undoped $LaFeO_3$, only the analysis on 0.47%Ru photocatalyst are reported, being similar the results obtained for all the others Ru-doped $LaFeO_3$ samples.

The SEM images show that the size of photocatalysts particles is not uniform due to agglomeration phenomena induced by particle–particle interactions. However, porous structure can be clearly seen in the SEM images, revealing the low density product, loose and porous material [57] due to the role of citric acid in the combustion of gel formed after the drying process at 130°C. In particular, at the combustion point, the citric acid generates gases
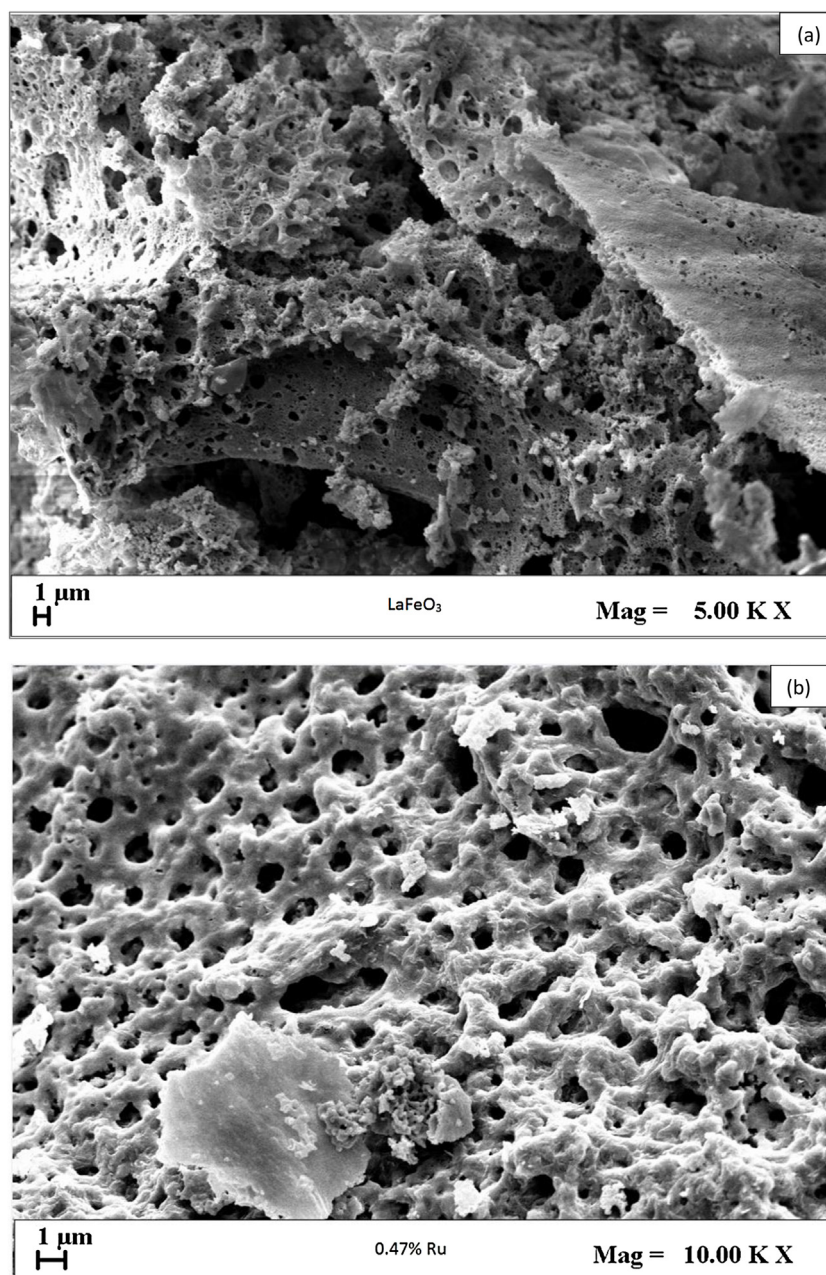
Fig. 6. SEM image of LaFeO$_3$ (a) and 0.47%Ru (b) photocatalysts.

that tried to come out from the gel by breaking the gel and generating the porous structure of LaFeO$_3$ (Fig. 6a) and Ru-doped LaFeO$_3$ (Fig. 6b) photocatalysts [57].

3.2. Photocatalytic activity results

3.2.1. Effect of Ru content on H$_2$ production and glucose degradation

During the dark phase, no product was detected in gaseous phase. Fig. 7 reports the behavior of glucose degradation and hydrogen production as a function of Ru loading obtained after 4 h of irradiation under UV-LEDs light at the spontaneous pH of the solution (pH = 6).

The hydrogen production was reported as the ratio between the µmoles produced and the catalyst amount (g$_{cat}$) used in the tests.

All the Ru-doped LaFeO$_3$ photocatalysts demonstrated a better activity compared to undoped LaFeO$_3$. The higher glucose degra-

dation (about 70%) was achieved for 0.47%Ru catalyst. Glucose degradation efficiency increased as Ru% was increased from 0.12 to 0.47 mol%, and decreased when Ru% was increased from 0.47 to 2.33 mol%, reaching a value lower also than pure LaFeO$_3$. In parallel, the same trend was observed for H$_2$ production with the higher value (2179 µmol/g$_{cat}$) achieved for 0.47%Ru after the same irradiation time. The observed H$_2$ production was higher than that one reported in the literature concerning the generation of hydrogen from the photocatalytic degradation of glucose on perovskites [41].

Ru^{3+} ions in the crystalline structure of the LaFeO$_3$ could act as electron scavengers preventing the holes–electrons (h$^+$/e$^-$) recombination, and consequently causing the enhancement of the photocatalytic activity [58]. This effect could be predominant for a Ru loading up to 0.47 mol%. The decreased efficiency observed when Ru% was increased from 0.47 to 2.33 mol% is probably due to the presence of RuO$_2$ on the catalyst surface (XRD analysis, Fig. 2). The presence of RuO$_2$ crystallites may reduce the light penetration,
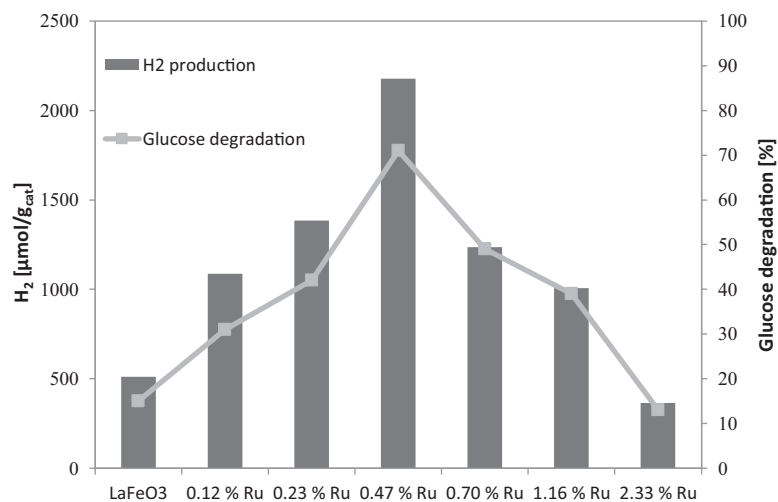
Fig. 7. Behavior of glucose degradation and hydrogen production after 4 h of irradiation for all the photocatalysts; light source: UV-LEDs; glucose initial concentration: 1000 mg/L; catalyst dosage: 1.5 g/L; solution volume: 80 mL.
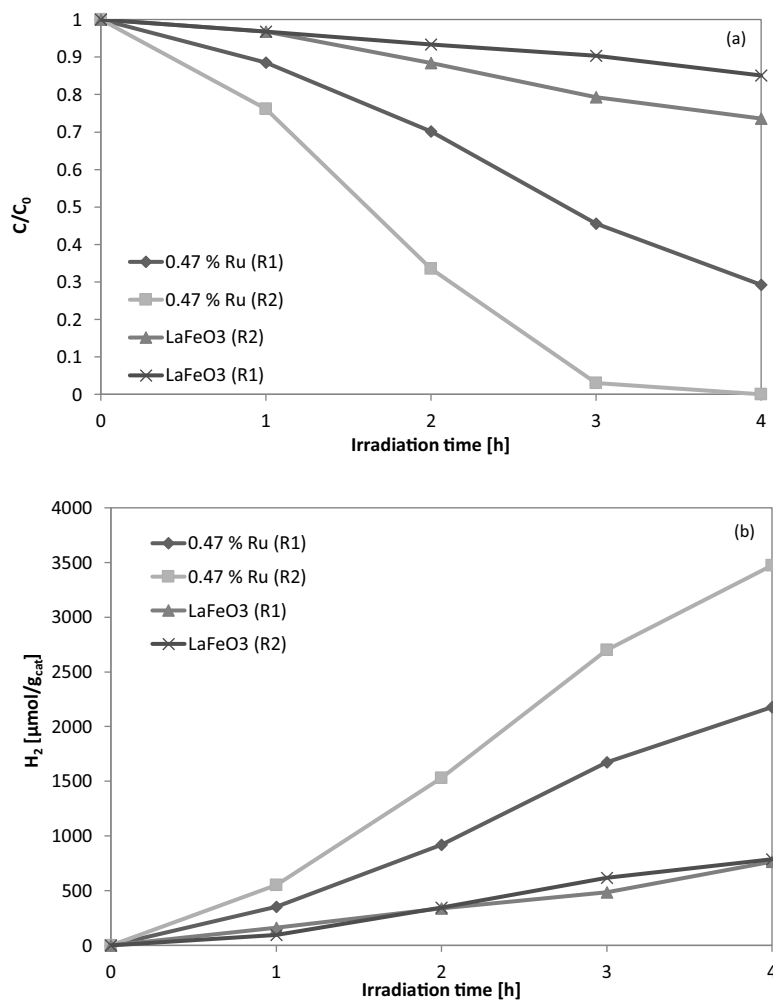

Fig. 8. Influence of reactor configuration on glucose degradation (a) and hydrogen production (b) with 0.47%Ru photocatalyst; light source: UV-LEDs; glucose initial concentration: 1000 mg/L; catalyst dosage: 1.5 g/L; solution volume: 80 mL.
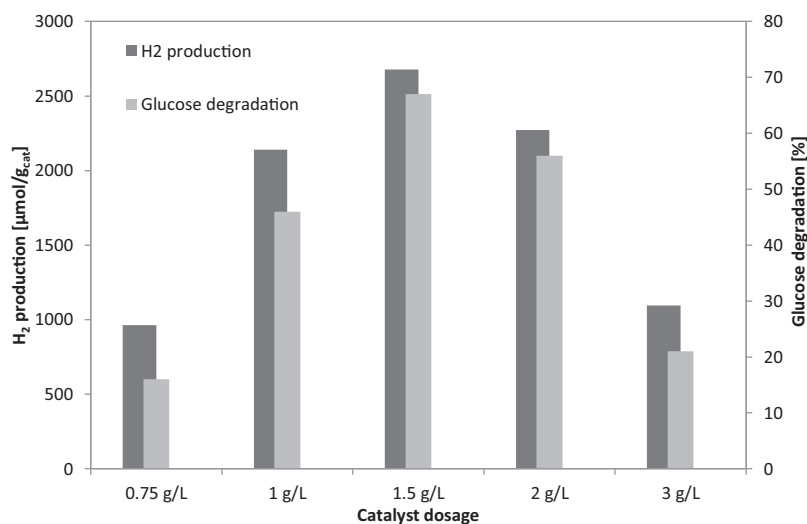
Fig. 9. Influence of catalyst dosage on glucose degradation and hydrogen production after 2 h of irradiation. Photocatalyst: 0.47%Ru; light source: UV-LEDs; glucose initial concentration: 1000 mg/L; photoreactor R2; solution volume: 80 mL.
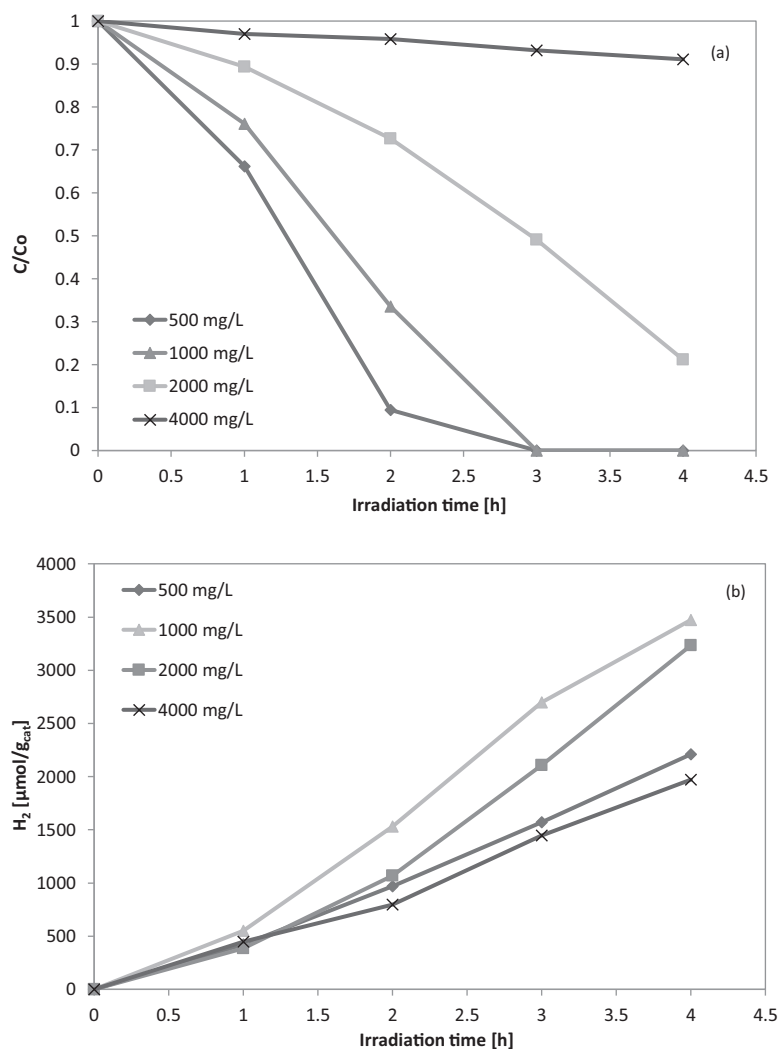

Fig. 10. Glucose degradation (a) and hydrogen production (b) as a function of irradiation time for different glucose initial concentrations. Photocatalyst: 0.47%Ru; light source: UV-LEDs; catalyst dosage: 1.5 g/L; photoreactor R2; solution volume: 80 mL.
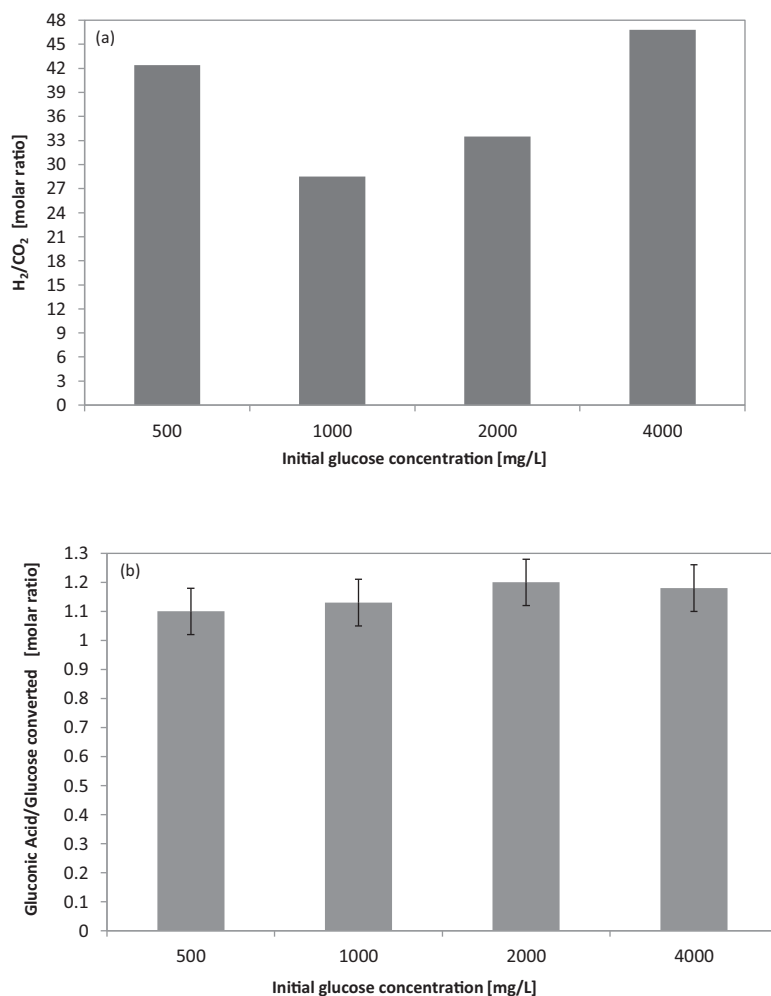
Fig. 11. Influence of initial glucose concentration on CO_2/H_2 molar ratio (a) and gluconic acid formed/glucose converted molar ratio (b) for different initial glucose concentrations; irradiation time: 4 h. Photocatalyst: 0.47%Ru; light source: UV-LEDs; catalyst dosage: 1.5 g/L; photoreactor R2; solution volume: 80 mL.
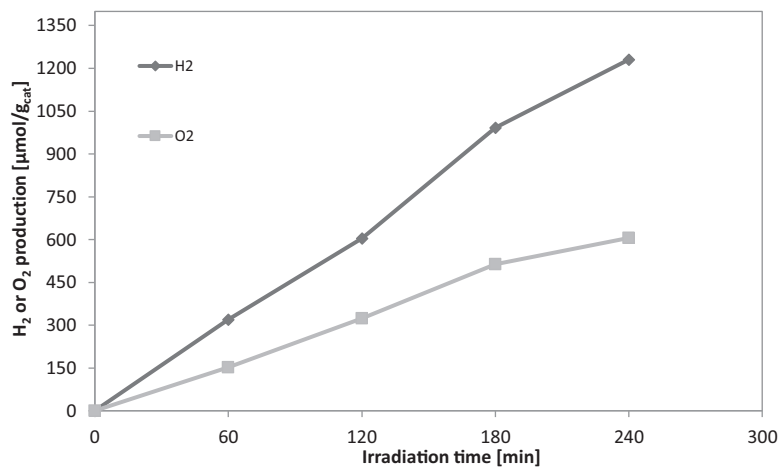

Fig. 12. Behavior of hydrogen and oxygen during the photocatalytic water splitting reaction. Photocatalyst: 0.47%Ru; light source: UV-LEDs; catalyst dosage: 1.5 g/L; photoreactor R2; solution volume: 80 mL.

retarding the activation of the photocatalyst and the generation of photoinduced charge carriers or can act as recombination centers diminishing the H_2 production and the glucose degradation [24,59].

The possible release of La and Ru was investigated by inductive coupled plasma-mass spectrometry analyzing the solution recov-

ered after the photocatalytic test on 0.47%Ru sample showing that no release of La nor Ru was detected.

According to these results 0.47 mol% of Ru loading was considered to be the optimal value for the studied reaction.
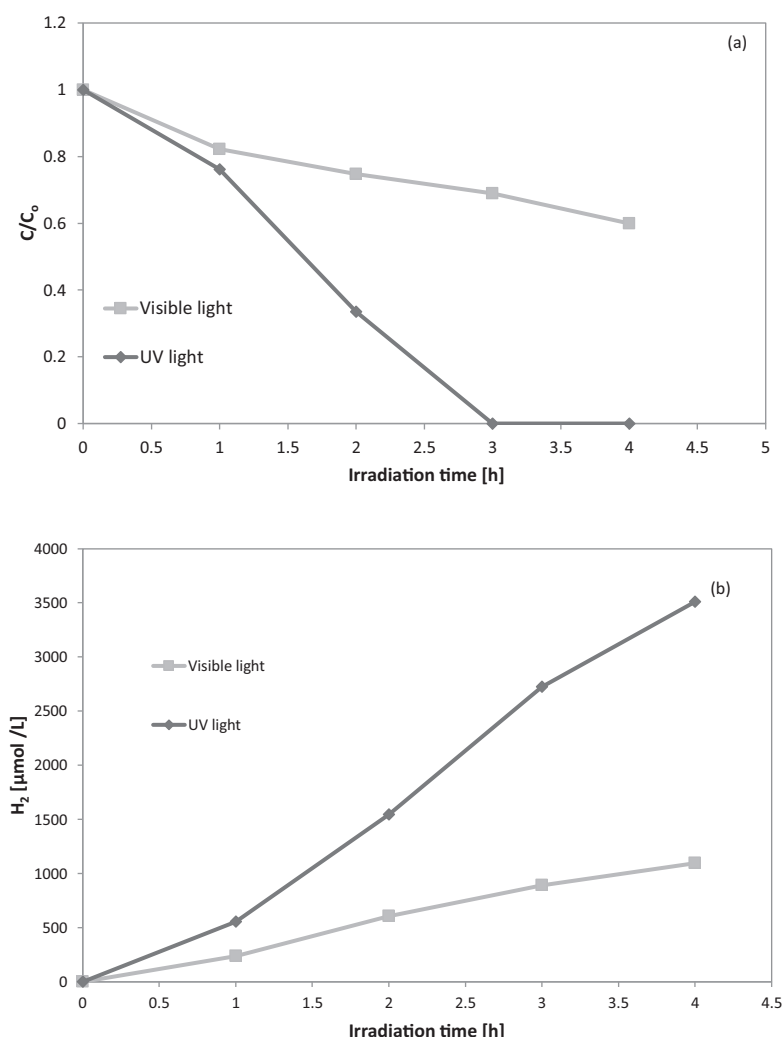
Fig. 13. Glucose degradation (a) and hydrogen production (b) during UV and visible light irradiation. Photocatalyst: 0.47%Ru; initial glucose concentration: 1000 mg/L; catalyst dosage: 1.5 g/L; photoreactor R2; solution volume: 80 mL.

3.2.2. Influence of the reactor configuration on the photocatalytic activity

The optimized photocatalyst (0.47%Ru) was used to investigate the influence of the reactor configuration. In particular a new set of experiments was carried out with the new reactor (R2) with a nominal volume equal to the first one (R1) but with an internal diameter equal to half (1.25 cm). The aim was to enhance the photonic transport by increasing the photons flow that intercepts the photocatalysts particles dispersed into the glucose solution. Fig. 8 shows the comparison in terms of photocatalytic activity between the two reactors. R2 resulted in a significantly higher glucose degradation compared to R1: in particular, an almost complete sugar degradation after 3 h of UV irradiation was observed for R2 compared to 70% removal in 4 h of UV irradiation observed for R1 (Fig. 8a). Noteworthy, glucose degradation had already reached about 70% after 2 h of irradiation in the experiments performed with the reactor R2. Moreover, in parallel, the hydrogen production (Fig. 8b) was higher with the photoreactor R2 (3474 μmol/L) compared to that one obtained with the photoreactor R1 (2179 μmol/g_{cat}).

These results are in agreement with a previous work where a similar photoreactor configuration was investigated in the removal of chemical oxygen demand (COD) of a highly polluted wastewater [48]. It is underlined that the percentage of irradiated catalyst volume is different. For an ID of 1.25 cm (photoreactor R2), it is larger than that obtained for an ID of 2.5 cm (photoreactor R1) indicating that the attenuation of the available light energy is a key parameter that affects the photocatalytic performances of the reactor [60,61].

3.2.3. Optimization of catalyst dosage for photocatalytic tests

The optimization of the catalyst dosage was carried out under UV irradiation with the photoreactor R2 by testing different dosages of 0.47%Ru photocatalyst, in the range 0.75–3 g/L. Photocatalytic efficiency increased as catalyst loading was increased up to 1.5 g/L (Fig. 9).

Further increase in catalyst loading resulted in a decreased degradation of glucose and lower H_2 production. Possibly, the increase in the catalyst dosage over the optimum value resulted in a decreased light penetration through the solution because of the increased opacity of the aqueous suspension [62].

3.2.4. Influence of initial glucose concentration

Fig. 10 shows the effect of the initial glucose concentration on both its degradation (Fig. 10a) and hydrogen production (Fig. 10b), under UV light. In particular, glucose degradation decreased as the initial concentration was increased. It is worthwhile to note that an increase of the hydrogen production was observed up to 1000 mg/L of initial concentration of glucose, in agreement with the results available in scientific literature [63].
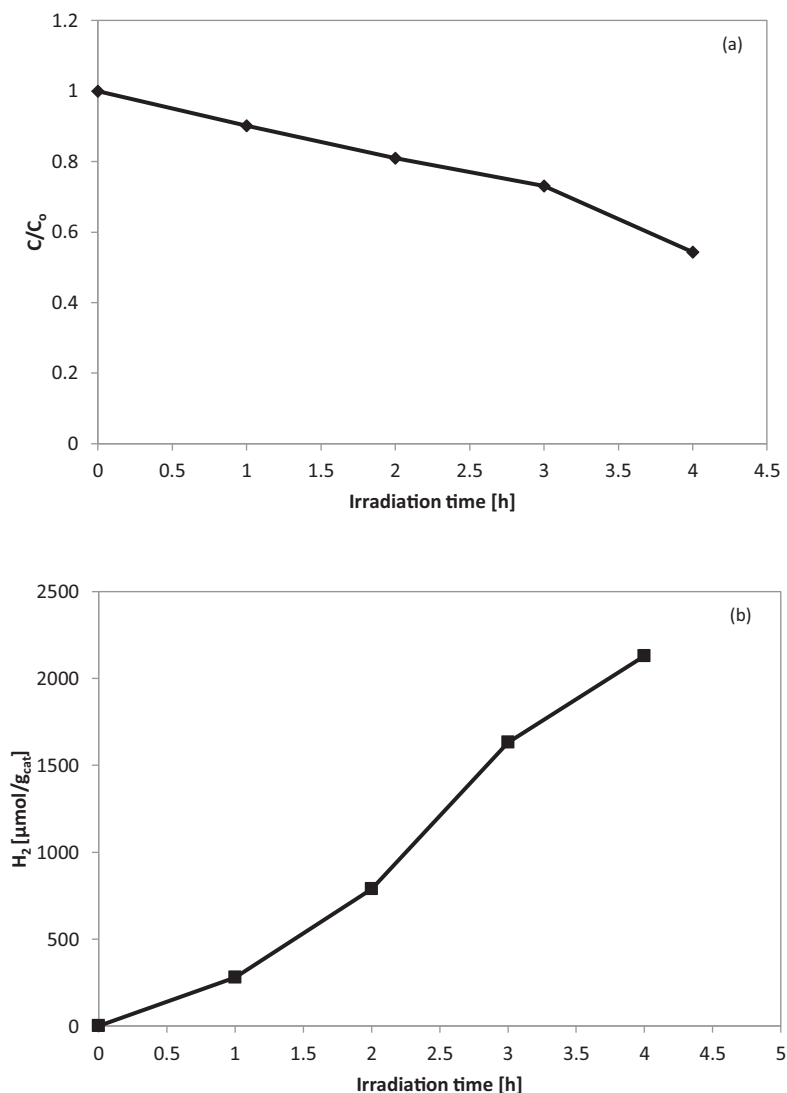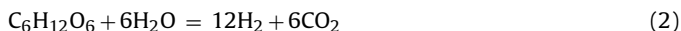
Fig. 14. Maltose degradation (a) and hydrogen production (b) from real wastewater. Photocatalyst: 0.47%Ru; light source: visible LEDs; catalyst dosage: 1.5 g/L; photoreactor R2; solution volume: 80 mL.

The H_2 production from glucose degradation could be obtained according to the sugar photoreforming reaction:

$$C_6H_{12}O_6 + 6H_2O = 12H_2 + 6CO_2 \qquad (2)$$

In this reaction the H_2/CO_2 ratio is equal to 2. However, in our case, the ratio H_2/CO_2 is in the range 28–46, as initial glucose concentration was varied, and never equal to 2 (Fig. 11a).

On the other hand, the analysis of the liquid phase showed that gluconic acid is formed during photocatalytic process and the ratio between the moles of gluconic acid produced and the moles of glucose converted is approximately equal to 1 for all the tested concentrations (Fig. 11b), according to a previous work on LaFeO$_3$ based photocatalysts [41].

Part of the additional CO_2 produced could come from the decarboxylation reaction of gluconic acid [64,65]. But, taking into account the results reported in Fig. 11a, this last reaction is expected to take place at a limited extend. On the basis of these observations and considering the behavior shown in Fig. 11b, H_2 and gluconic acid could be mainly produced from the photocatalytic degradation of glucose, according to the following reaction:

$$C_6H_{12}O_6 + H_2O = H_2 + C_6H_{12}O_7 \qquad (3)$$

3.2.5. Water splitting reaction on 0.47%Ru photocatalyst

The ability of 0.47%Ru photocatalyst in the hydrogen production through water splitting reaction (without glucose) under UV irradiation was also evaluated. The results are reported in Fig. 12.

The production of hydrogen and oxygen progressively increased as irradiation time increased. Moreover, the H_2/O_2 ratio was about 2. This result confirms that hydrogen is produced from water splitting according the following reaction:

$$H_2O = H_2 + \tfrac{1}{2}O_2 \qquad (4)$$

It is worthwhile to note that the amount of hydrogen reached a value of 1230 μmol/g$_{cat}$ (after 4 h of irradiation), significantly lower than that obtained in presence of glucose. In fact, to promote photocatalytic water splitting, various oxidizing sacrificial agents have been added to water; the role of sacrificial agent is to scavenge the coproduced O_2 due to water splitting, and, thus, to prevent the reverse reaction of O_2 with H_2 to H_2O [23,66]. Typically, the sacrificial compounds are hydrocarbons such as saccharides, alcohol and acetic acid [67]. However it must be taken into account that, in our case, the water splitting reaction plays an important role in the photocatalytic hydrogen production.

3.3. Photocatalytic activity of 0.47%Ru under visible light irradiation

The effect of different light sources (UV or visible LEDs) was evaluated on the 0.47%Ru catalyst (Fig. 13), which showed the best performances. According to UV–vis DRS results (Table 1), this catalyst was expected to be active also in the presence of visible light (band-gap equal to 1.98 eV). In particular, the photocatalytic experiment was carried out with a solution containing 1000 mg/L of glucose, a catalyst dosage equal to 1.5 g/L and the optimized R2 configuration. The observed glucose degradation was equal to 40% after 4 h of visible light irradiation (Fig. 13a) and the hydrogen production was equal to 1098 μmol/g_{cat} (Fig. 13b) after the same irradiation time. These results, also if lower than that obtained in presence of UV light, confirm the activity of the optimized photocatalyst also in presence of visible light irradiation.

3.4. Photocatalytic hydrogen production from real wastewater with 0.47%Ru catalyst under visible light

Since the investigated photocatalytic process was really effective in the hydrogen production from glucose-containing solutions, the effect of the phtocatalyst 0.47% Ru was also investigated in the treatment and valorization of real wastewater from brewing process (supplied by an Italian company producing beer) (Fig. 14). the wastewater sample was filtered before the photocatalytic process to remove the suspended solids. Typically the main component of this type of wastewater is maltose ($C_{12}H_{22}O_{11}$), a sugar of the family of glucides disaccharides, consisting of two glucose molecules bonded by an oxygen atom [66]. The degradation of maltose during photocatalytic process (visible light) was evaluated by measuring absorbance changes at the wavelength of 268 nm (Fig. 14a).

After 4 h of visible light irradiation, a degradation of maltose equal to 50% was observed. In parallel photocatalytic hydrogen production reached the value of about 2128 μmol/g_{cat} within four hours of irradiation (Fig. 14b). These results confirm the applicability of the photocatalytic process also to a real wastewater and the possibility to valorize the wastewater obtaining hydrogen from the degradation of maltose under visible light.

4. Conclusions

Non-doped and Ru-doped $LaFeO_3$ nanoparticles were successfully synthesized by the solution combustion synthesis method. Characterization results showed the formation of orthorhombic perovskite type structure and that Ru^{3+} cation partially substitutes Fe^{3+} cation in the perovskite structure. Moreover the absorption edge of Ru-doped $LaFeO_3$ catalysts has a red shift and also a stronger absorption than the pure $LaFeO_3$ in the visible region due to the electronic transition from donor levels formed with Ru^{3+} to the conduction band of the host perovskite structure.

The highest photocatalytic glucose degradation and hydrogen production was observed for 0.4 mol% Ru-doped $LaFeO_3$ sample (0.47%Ru). Ru^{3+} in the crystalline structure of the $LaFeO_3$ could act as electron scavengers preventing the holes–electrons recombination, and consequently causing the enhancement of the photocatalytic activity. For Ru content higher than 0.47 mol%, the photocatalytic activity decreased because of the presence of RuO_2 on the catalyst surface. Therefore 0.47 mol% of Ru loading is considered to be an optimal value for the studied reaction. In particular, after 4 h of UV irradiation with 0.47%Ru, glucose degradation and hydrogen production were equal to 70% and 2179 μmol/g_{cat}, respectively.

Moreover the effect of the reactor configuration on the hydrogen production and degradation of glucose was assessed. The results showed that with the same volume but reducing the diameter of the photocatalytic reactor from 2.5 to 1.25 cm, the photonic transport was enhanced and consequently the activity of the 0.47%Ru increased. In particular, under UV light, the hydrogen production passed from 2179 to 3474 μmol/g_{cat} and the glucose degradation was complete after 3 h of irradiation.

The optimized 0.47%Ru has shown high efficiency also under visible light obtaining about 40% of glucose degradation after 4 h of irradiation and a hydrogen production equal to 1919 μmol/L. Finally the efficiency of 0.47%Ru photocatalyst under visible light was also tested on a real wastewater from the brewing process; the results showed a hydrogen production equal to 2128 μmol/g_{cat} in 4 h of irradiation denoting a good performance of the optimized photocatalytic system also for the treatment of real wastewater with the aim to obtain the simultaneously degradation and valorization (through hydrogen production) of organic pollutants.

References

[1] V.M. Daskalaki, D.I. Kondarides, Catal. Today 144 (2009) 75–80.
[2] M. De Oliveira Melo, L.A. Silva, J. Braz. Chem. Soc. 22 (2011) 1399–1406.
[3] E.A. Sánchez, M.A. D'Angelo, R.A. Comelli, Int. J. Hydrogen Energy 35 (2010) 5902–5907.
[4] R. Hashaikeh, I.S. Butler, J.A. Kozinski, Energy Fuels 20 (2006) 2743–2747.
[5] S. Authayanun, A. Arpornwichanop, W. Paengjuntuek, S. Assabumrungrat, Int. J. Hydrogen Energy 35 (2010) 6617–6623.
[6] A.T. Marshall, R.G. Haverkamp, Int. J. Hydrogen Energy 33 (2008) 4649–4654.
[7] R. Abe, J. Photochem. Photobiol. C: Photochem. Rev. 11 (2010) 179–209.
[8] J.J. Murcia, M.C. Hidalgo, J.A. Navio, V. Vaiano, D. Sannino, P. Ciambelli, Catal. Today 209 (2013) 164–169.
[9] D. Sannino, V. Vaiano, P. Ciambelli, Catal. Today 205 (2013) 159–167.
[10] V. Vaiano, O. Sacco, D. Sannino, P. Ciambelli, Chem. Eng. J. 261 (2015) 3–8.
[11] V. Vaiano, D. Sannino, P. Ciambelli, Photochem. Photobiol. Sci. 14 (2015) 550–555.
[12] M. Bellardita, E.I. García-López, G. Marcì, L. Palmisano, Int. J. Hydrogen Energy (2016).
[13] A.L. Luna, E. Novoseltceva, E. Louarn, P. Beaunier, E. Kowalska, B. Ohtani, M.A. Valenzuela, H. Remita, C. Colbeau-Justin, Appl. Catal. B: Environ. 191 (2016) 18–28.
[14] I. Majeed, M.A. Nadeem, M. Al-Oufi, M.A. Nadeem, G.I.N. Waterhouse, A. Badshah, J.B. Metson, H. Idriss, Appl. Catal. B: Environ. 182 (2016) 266–276.
[15] A. Meng, J. Zhang, D. Xu, B. Cheng, J. Yu, Appl. Catal. B: Environ. 198 (2016) 286–294.
[16] G.L. Chiarello, E. Selli, Adv. Hydrogen Prod. Storage Distrib. (2014) 216–247.
[17] X. Li, J. Yu, L. Low, Y. Fang, J. Xiao, X. Chen, J. Mater. Chem. A 3 (2015) 2485–2534.
[18] T. Di, B. Zhu, J. Zhang, B. Cheng, J. Yu, Appl. Surf. Sci. 389 (2016) 775–782.
[19] J. Yu, Y. Yu, P. Zhou, W. Xiao, B. Cheng, Appl. Catal B 156–157 (2014) 184–191.
[20] Y. Xu, R. Xu, Appl. Surf. Sci. 351 (2015) 779–793.
[21] L. Lu, M. Lv, G. Liu, X. Xu, Appl. Surf. Sci. (2016), Ahead of Print.
[22] E.A. Kozlova, A.V. Vorontsov, Int. J. Hydrogen Energy 35 (2010) 7337–7343.
[23] B. Zieliñska, E. Borowiak-Palen, R.J. Kalenczuk, Int. J. Hydrogen Energy 33 (2008) 1797–1802.
[24] M. Antoniadou, V. Vaiano, D. Sannino, P. Lianos, Chem. Eng. J. 224 (2013) 144–148.
[25] M. Serra, H.G. Baldovi, F. Albarracin, H. Garcia, Appl. Catal. B 183 (2016) 159–167.
[26] Y. Li, J. Wang, S. Peng, G. Lu, S. Li, Int. J. Hydrogen Energy 35 (2010) 7116–7126.
[27] W. Deng, Q. Zhang, Y. Wang, Catal. Today 234 (2014) 31–41.
[28] V. Vaiano, G. Iervolino, G. Sarno, D. Sannino, L. Rizzo, J.J. Murcia Mesa, M.C. Hidalgo, J.A. Navío, Oil Gas Sci. Technol. 70 (2015) 891–902.
[29] Y. Li, D. Gao, S. Peng, G. Lu, S. Li, Int. J. Hydrogen Energy 36 (2011) 4291–4297.
[30] M. Zhou, Y. Li, S. Peng, G. Lu, S. Li, Catal. Commun. 18 (2012) 21–25.
[31] M. Jiménez-Tototzintle, I. Oller, A. Hernández-Ramírez, S. Malato, M.I. Maldonado, Chem. Eng. J. 273 (2015) 205–213.
[32] J. Schneider, M. Matsuoka, M. Takeuchi, J. Zhang, Y. Horiuchi, M. Anpo, D.W. Bahnemann, Chem. Rev. (Washington, DC, U. S.) 114 (2014) 9919–9986.
[33] M.C. Wu, I.C. Chang, W.K. Huang, Y.C. Tu, C.P. Hsu, W.F. Su, Thin Solid Films 570 (2014) 371–375.
[34] F. Sordello, C. Minero, Appl. Catal. B 163 (2015) 452–458.
[35] Y. Li, Y. Xie, S. Peng, G. Lu, S. Li, Chemosphere 63 (2006) 1312–1318.
[36] Y. Li, G. Lu, S. Li, Appl. Catal. A: Gen. 214 (2001) 179–185.
[37] Y. Li, G. Lu, S. Li, J. Photochem. Photobiol. A: Chem. 152 (2002) 219–228.
[38] A. Patsoura, D.I. Kondarides, X.E. Verykios, Appl. Catal. B: Environ. 64 (2006) 171–179.
[39] J. Yang, R. Hu, W. Meng, Y. Du, Chem. Commun. (Cambridge U. K.) 52 (2016) 2620–2623.
[40] S. Li, L. Jing, W. Fu, L. Yang, B. Xin, H. Fu, Mater. Res. Bull. 42 (2007) 203–212.
[41] G. Iervolino, V. Vaiano, D. Sannino, L. Rizzo, P. Ciambelli, Int. J. Hydrogen Energy 41 (2016) 959–966.

[42] I. Natali Sora, F. Fontana, R. Passalacqua, C. Ampelli, S. Perathoner, G. Centi, F. Parrino, L. Palmisano, Electrochim. Acta 109 (2013) 710–715.
[43] L. Malavasi, M.C. Mozzati, C. Tealdi, C.B. Azzoni, G. Flor, J. Phys. Chem. B 109 (2005) 20707–20713.
[44] Y. Hwang, D.S. Kang, M.H. Park, J. Ceram. Process. Res. 11 (2010) 397–400.
[45] J.J. Murcia, M.C. Hidalgo, J.A. Navío, V. Vaiano, D. Sannino, P. Ciambelli, Catal. Today 209 (2013) 164–169.
[46] O. Sacco, V. Vaiano, C. Han, D. Sannino, D.D. Dionysiou, Appl. Catal. B: Environ. 164 (2015) 462–474.
[47] P. Ciambelli, D. Sannino, V. Palma, V. Vaiano, R.S. Mazzei, P. Eloy, E.M. Gaigneaux, Catal. Today 141 (2009) 367–373.
[48] V. Vaiano, O. Sacco, M. Stoller, A. Chianese, P. Ciambelli, D. Sannino, Int. J. Chem. Reactor Eng. 12 (2014).
[49] V. Vaiano, O. Sacco, D. Sannino, P. Ciambelli, Appl. Catal. B: Environ. 170–171 (2015) 153–161.
[50] M. Dubois, K.A. Gilles, J.K. Hamilton, P.A. Rebers, F. Smith, Anal. Chem. 28 (1956) 350–356.
[51] S.N. Tijare, M.M. Joshi, S.S. Rayulu, N.K. Labhasetwar, Photocatalytic hydrogen generation through water splitting on nano-crystalline LaFeO3 perovskite, ACS Natl. Meet. Book Abs. (2010).
[52] M. Senthilnanthan, D.P. Ho, S. Vigneswaran, H.H. Ngo, H.K. Shon, Sep. Purif. Technol. 75 (2010) 415–419.
[53] H.R. Gurav, R. Bobade, V.L. Das, S. Chilukuri, Indian J. Chem. Sect. A: Inorg. Bio-inorg. Phys. Theor. Anal. Chem. 51A (2012) 1339–1347.
[54] K.M. Parida, K.H. Reddy, S. Martha, D.P. Das, N. Biswal, Int. J. Hydrogen Energy 35 (2010) 12161–12168.
[55] L. Hou, G. Sun, K. Liu, Y. Li, F. Gao, J. Sol-Gel Sci. Technol. 40 (2006) 9–14.
[56] W. Wang, M.O. Tadé, Z. Shao, Chem. Soc. Rev. 44 (2015) 5371–5408.
[57] S.M. Khetre, H.V. Jadhav, S.R. Bamane, Rasayan. J. Chem. 3 (2010) 82–86.
[58] R.A. Elsalamony, S.A. Mahmoud, Arab. J. Chem. (2012).
[59] T.D. Nguyen-Phan, S. Luo, D. Vovchok, J. Llorca, J. Graciani, J.F. Sanz, S. Sallis, W. Xu, J. Bai, L.F.J. Piper, D.E. Polyansky, E. Fujita, S.D. Senanayake, D.J. Stacchiola, J.A. Rodriguez, ACS Catal. 6 (2016) 407–417.
[60] M.G. Chiovetta, R.L. Romero, A.E. Cassano, Chem. Eng. Sci. 56 (2001) 1631–1638.
[61] V. Palma, D. Sannino, V. Vaiano, P. Ciambelli, Ind. Eng. Chem. Res. 49 (2010) 10279–10286.
[62] V. Vaiano, G. Iervolino, D. Sannino, J.J. Murcia, M.C. Hidalgo, P. Ciambelli, J.A. Navío, Appl. Catal. B: Environ. 188 (2016) 134–146.
[63] X. Fu, J. Long, X. Wang, D.Y.C. Leung, Z. Ding, L. Wu, Z. Zhang, Z. Li, X. Fu, Int. J. Hydrogen Energy 33 (2008) 6484–6491.
[64] M.R. Hoffmann, S.T. Martin, W. Choi, D.W. Bahnemann, Chem. Rev. (Washington, D. C.) 95 (1995) 69–96.
[65] G. Iervolino, V. Vaiano, J.J. Murcia, L. Rizzo, G. Ventre, G. Pepe, P. Campiglia, M.C. Hidalgo, J.A. Navío, D. Sannino, J. Catal. 339 (2016) 47–56.
[66] T. Kawai, T. Sakata, Nature (London) 286 (1980) 474–476.
[67] S. Deguchi, T. Takeichi, S. Shimasaki, M. Ogawa, N. Isu, AIChE J. 57 (2011) 2237–2243.